Fabrication of Self-assembling Nanofibers with Optimal Cell Uptake and Therapeutic Delivery Efficacy

*Dawei Xu[1], Damien S. K. Samways[2], He Dong[1,]**

[1]Department of Chemistry & Biomolecular Science, Clarkson University, Potsdam, USA.

[2]Department of Biology, Clarkson University, Potsdam, USA

Keywords: supramolecular assembly; cell penetrating peptide; drug delivery; cell uptake; membrane activity

*Corresponding author: Dr. He Dong
Department of Chemistry & Biomolecular Science, Clarkson University, Potsdam, NY 13699. USA, E-mail address: hdong@clarkson.edu

Abstract

Effective strategies to fabricate finite organic nanoparticles and understanding their structure-dependent cell interaction is highly important for the development of long circulating nanocarriers in cancer therapy. In this contribution, we will capitalize on our recent development of finite supramolecular nanofibers based on the self-assembly of modularly designed cationic multidomain peptides (MDPs) and use them as a model system to investigate structure-dependent cell penetrating activity. MDPs self-assembled into nanofibers with high density of cationic charges at the fiber-solvent interface to interact with the cell membrane. However, despite the multivalent charge presentation, not all fibers led to high levels of membrane activity and cellular uptake. The flexibility of the cationic charge domains on self-assembled nanofiber plays a key role in effective membrane perturbation. Nanofibers were found to sacrifice their dimension, thermodynamic and kinetic stability for a more flexible charge domain in order to achieve effective membrane interaction. The increased membrane activity led to improved cell uptake of membrane-impermeable chemotherapeutics through membrane pore formation. *In vitro* cytotoxicity study showed co-administering of water-soluble doxorubicin with membrane-active peptide nanofibers dramatically reduced the IC50 by eight folds compared to drug alone. Through these detailed structure and activity studies, the acquired knowledge will provide important guidelines for the design of a variety of supramolecular cell penetrating nanomaterials not limited to peptide assembly which can be used to probe various complex biological processes.

Table of Content

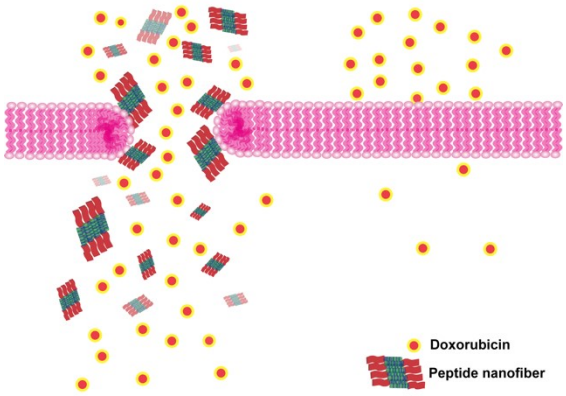

1. Introduction

Supramolecular assembly of peptides has been widely used as a bottom-up approach to generate functional nanomaterials [1-5]. These materials exhibit well-defined molecular structure, internal ordering and nanostructure, which were found to be important factors to manipulate their interactions with cells and tissues [6-11]. Fundamental understanding the relationship between molecular/supramolecular nanostructure and bioactivity of these assemblies is crucial to develop self-assembled peptides with optimized biological properties. In the last two decades, structure-activity correlation has been primarily focused on peptide nanofibers of infinite dimension for tissue engineering application [12-17]. It came to realization that the impact of finite peptide nanostructures could also be far-reaching particularly for the development of systemic therapeutic delivery vehicles where the length scale of the assembly plays important roles for cell uptake and tissue penetration as dictated by the enhanced permeation retention (EPR) effect. There have been numerous studies on the design of inorganic [18-21], polymeric [22-25], and protein-based rod-like nanoparticles [26-30] as long-circulating anisotropic nanocarriers. However, limited research was reported on finite anisotropic nanomaterials based on rationally designed and engineered peptide assembly. The lack of related research is partly due to the difficulty of fabricating peptide nanofibers with precisely controlled morphology, optimally below 100 nm that can potentially be used as long circulating nanocarriers. Notably, supramolecular peptides may also overcome some of the intrinsic limitations associated with single chain peptides, e.g. stability to greatly expand their biomedical utility [31-34].

We have been dedicating to the development of water-soluble finite supramolecular peptide nanostructures with built-in biological functions and understanding their sequence-structure-activity correlation on both the molecular and supramolecular level [31-35]. Self-assembling

Antimicrobial Nanofibers (SAANs) [32] and Filamentous Cell Penetrating Peptides (FCPPs) [31, 34] are two families of supramolecular peptides that we developed to mimic natural antimicrobial peptides and cell penetrating peptides respectively with dramatically improved stability, bioactivity and cytocompatibility. In particular, FCPPs were designed and fabricated as a highly effective gene delivery system based on the self-assembly of *de novo* designed cationic β-sheet forming multi-domain peptides (MDPs) [31]. In our previous study, we compared the cell penetrating activity of nanofiber forming peptides with their monomeric analogue [34], showing the important role of nanofiber formation in increasing peptides' membrane activity. In the current work, we seek to understand the structure-activity relationship (SAR) of these peptide nanofibers and identify critical structural features governing the cell penetrating activity of these assemblies. Despite the multivalent charge presentation, not all fibers led to high levels of membrane activity and cellular uptake. The interaction between peptides and the cell membrane is governed by combined chemical and physical parameters and the flexibility of the cationic charge domains on self-assembled nanofiber is critically important for effective membrane perturbation. Nanofibers were found to sacrifice their dimension, thermodynamic and kinetic stability for a more flexible charge domain in order to achieve effective membrane interaction and therapeutic delivery efficacy. We believe rational design of peptide building blocks to form FCPPs and detailed understanding of their molecular and supramolecular nanostructure and their effect on biological activity is crucial for the development of highly effective supramolecular cell penetrating peptides. The fundamental knowledge showed here can also be applied to the design of other types of protein/polymeric cell penetrating nanomaterials which can be used to probe various complex biological processes.

2. Materials and methods

2.1 Materials

MBHA rink amide resin, Fmoc-protected amino acids, O-(Benzotriazol-1-yl)-N,N,N',N'-tetramethyluronium hexafluorophosphate (HBTU) were purchased from Novabiochem. Piperidine and diisopropylethylamine (DIPEA) was purchased from Sigma-Aldrich. All other reagents and solvents for peptide synthesis and purification were purchased from Fisher Scientific and used as received. Desalting column VariPure IPE was ordered Agilent Technologies (Apple Valley, MN). Dulbecco's modified Eagle medium (DMEM) culture medium, hoechst 33342 and LysoTracker Red DND-99 was purchased from Life Technologies. Fetal Bovine Serum (FBS) was ordered from VWR (Radnor, PA). CCK8 assay kit was ordered from Dojindo Molecular Technologies (Rockville, MD). Fluorescence measurements were performed on Varian Cary Eclipse fluorescence spectrophotometer. Reversed-phase HPLC was carried out using HITACHI L-7100 pump. UV absorbance was measured on a micro-plate reader (Vitor2 1420 Multilabel Counter, PerkinElmer) for cell toxicity experiment.

2.2 Peptide synthesis and purification

The synthesis of MDPs followed standard Fmoc-solid phase peptide synthesis method. Briefly, Fmoc group was removed with 20% piperidine/DMF (V/V) for five minutes and the deprotection reaction was repeated once. Fmoc-protected amino acids (5 eq), coupling reagent, HBTU (5 eq) and diethylpropylamine (10 eq) were added to the solid resin and the couple reaction run for 45 mins. Upon completion of the synthesis, the N-terminus of the peptide was capped with acetic anhydride in the presence of DIPEA in DMF for 1 hr and the completion of acetylation reaction was confirmed by Kaiser test. Cleavage cocktail including trifluoroacetic acid (TFA) / triisopropylsilane (TIS) / H_2O (95/2.5/2.5 by volume) was added to the resin and mixed for 3 hrs. Cleavage solution was collected and the resin was rinsed with neat TFA for two times. Excessive

TFA was evaporated by air blow and residual peptide-TFA mixture was triturated with cold diethyl ether. Precipitates were isolated by centrifugation and washed with cold diethyl ether for three times. Peptide powder was dried under vacuum overnight before HPLC purification. A linear gradient of a binary water/acetonitrile solvent containing 0.05% TFA was used for HPLC purification on a preparative reverse phase C18 column. HPLC fraction was collected, combined and desalted to remove residual TFA salts. The desalted peptide solution was frozen in liquid nitrogen and lyophilized for 3 days. Mass was confirmed by MALDI-TOF. Expected mass for K10: 3225.80, Experimental result: 3226.10. Expected mass for K6: 2713.40, Experimental result: 2712.34. Expected mass for D-K10: 3225.80, Experimental result: 3228.99.

2.3 Critical aggregation concentration (CAC) measurement

CACs were determined using a previous protocol based on the fluorescence intensity change of tryptophan [35, 36]. Fluorescence measurements were performed at room temperature by monitoring the emission spectrum of peptides between 295 nm and 440 nm using an excitation wavelength at 280 nm. Peptide stock solution (160 μM) was added in 200 μL Tris buffer (20 mM, pH=7.5) with an increment of 2 μl each time. Fluorescence intensity at 350 nm was plotted as a function of peptide concentration. The CAC was determined at the concentration in which onset of nonlinearity was observed.

2.4 Fluorescence recovery experiment for kinetic stability measurement

Both FITC-labeled and non-labeled peptides were dissolved in Tris buffer (20 mM, pH=7.5) separately and incubated overnight before further use. FITC-Labeled peptides were prepared at a concentration of 15 μM and the non-labeled peptides were prepared at a concentration of 3 mM. The two solutions were mixed at a molar ratio of 1: 40. Time-dependent fluorescence intensity was recorded every 30 seconds for 24 hrs with the excitation wavelength at 497 nm and emission

at 527 nm. The excitation slit was set to 2.5 nm and emission slit was set to 2.5 nm. The subunit exchange rate was estimated by fitting the experimental data into two-rate first order kinetic equation.

2.5 Patch clamp electrophysiology

For patch clamp electrophysiology experiments, HEK293 cells were seeded onto glass coverslips, and transferred to a bath positioned on the stage of an inverted Olympus IX51 microscope. Cells were continuously perfused with a divalent-free extracellular solution containing 140 mM NaCl, 10 mM glucose, 10 mM HEPES, (pH adjusted to 7.4 with NaOH). Peptide solution was diluted in divalent-free extracellular solution to reach a final concentration of 16 μM for K10 and 26 μM for K6. Single cell current recordings were made in the broken patch whole cell voltage clamp configuration according to conventional methods [37] using low resistance (0.5-3 MΩ) borosilicate glass electrodes. Membrane potential was held at -40 mV for the duration of the experiment. Current recordings were sampled at 20 kHz and filtered at 5 KHz using an AxoPatch 200B amplifier (Molecular Devices) and digitized via a 1440 Digidata (Molecular Devices). The MDPs were applied using a Perfusion Fast-Step System SF-77 (Warner Instruments). Data was analyzed offline using IGOR Pro (Wavemetrics, Inc) software.

2.6 Cytotoxicity measurement

HeLa cells were seeded onto a 96-well plate at a density of 10^4 cells/well. 10 μl of peptide solution was added into cell culture to reach a final concentration of 16 μM for K10 and 26 μM for K6 to keep the overall charges equivalent. After 24 hrs of incubation, CCK-8 assay was used for cell viability measurement by monitoring UV absorbance at 450 nm. All the experiments were performed in four replicates and data was processed using Prism 6. For evaluation of cytotoxicity of mixed formulation containing peptides and DOX, DOX was first added into each well plate to

reach final concentrations at 1 μM, 10 μM, 100 μM, respectively. Peptides were added to the cell culture to reach a final concentration of 16 μM for K10 and 26 μM for K6. After 1 hr, 8 hrs and 24 hrs of incubation, cell viability was determined by CCK-8 assay according to the manufacturer's protocol. The optical absorbance of each well plate was measured on a microplate reader at the wavelength of 450 nm. All the experiments were performed in four replicates and data was processed using Prism 6.

2.7 Cell uptake

HeLa cells were seeded onto a confocal dish at a density of 1 x 10^5 cells/well. FITC-labeled peptides were prepared at a concentration of 160 μM in Tris buffer and incubated at room temperature overnight before further use. 20 μL of the peptide stock solution was added to the cell culture to reach a final peptide concentration of 16 μM. After 2 hrs and 24 hrs of incubation, cells were washed with PBS buffer for three times. Images were captured using a laser scanning confocal microscope (Leica DMi8, Germany) and processed with ImageJ software. For flow cytometry measurement, HeLa cells were seeded onto a 24-well plate at a density of 1 x 10^5 cells/well and cultured for 24 hrs before further use. DMEM medium was replaced and 20 μL of FITC-labeled peptide solutions were added to reach a final peptide concentration of 16 μM. After incubation with FITC-labeled MDPs for 2 hrs and 24 hrs, cells were washed with PBS buffer for three times. Cells were harvested with trypsin and washed twice with PBS buffer. 2% paraformaldehyde was used for cell fixation for 10 min. Cell uptake of the FITC-labeled peptide was quantified using a BD FACS Calibur flow cytometer. A minimum of 10,000 events per sample was analyzed and data was processed using FlowJo software.

2.7 Statistical analysis

All data were expressed as means ± standard deviation (SD). The statistical analysis was performed using Student's T-test and one-way analysis of variance (ANOVA) at confidence levels of 95% and 99% (Prism 6).

3. Results and discussion

3.1 Peptide design

The work presented here is inspired by our recent study that fiber-forming peptides, compared to their constitutional isomeric monomers, have greatly improved membrane activity and ability to deliver chemotherapeutics across the cell membrane [34]. As a follow-up study, a logical question to ask is "can all cationic peptide nanofibers be as effective to perturb the cell membrane for chemotherapeutics delivery?" Toward this goal, we initially synthesized four MDPs that have a general sequence of $K_x(QW)_6$ (x=2, 6, 10, 15) containing consecutive numbers of lysine residues to mimic the cell penetrating function and an alternating pattern of six hydrophilic (Q) and hydrophobic amino acids (W) repeating units to drive the formation of β-sheets nanofiber. Based on the design principle of "Molecular Frustration" [38], the length of the supramolecular nanofiber is dictated by the balance of the attractive interaction between the $(QW)_6$ units and repulsive interaction among the lysine residues. As the number of lysine residues increases, electrostatic repulsion shifts the assembly equilibrium and leads to fiber length reduction. It would be expected that self-assembly of these MDPs will result in nanofibers of different dimension and charge domain flexibility. In the current study, we are primarily interested in peptide nanofibers with lengths below 100 nm which may be more effective for passive tumor targeting due to the EPR effect [39-41]. It was found that $K_2(QW)_6$ was only slightly soluble in aqueous solution, forming crosslinked fiber network, therefore does not fit the purpose of the current study and was excluded in the initial evaluation. The remaining peptides were characterized by conventional

stained transmission electron microscopy (TEM) showing nanofibers formed by $K_{10}(QW)_6$ and $K_{15}(QW)_6$ had a subtle difference in terms of fiber length, while $K_6(QW)_6$ self-assembled into nanofibers that are significantly distinct from $K_{10}(QW)_6$ and $K_{15}(QW)_6$. Due to the above reasons, we selected $K_6(QW)_6$, termed as K6 and $K_{10}(QW)_6$, termed as K10 as representative peptide sequences that have similar chemical composition, yet can generate nanofibers of distinct morphology to further study and compare their structure-dependent biological activity. K10 peptide containing all D amino acids (termed as ^{d}K10) was also synthesized to further validate the design principle and confirm the SAR observed in the L-amino acid systems where their enzymatic stability may pose a practical challenge for future *in vivo* application. To note, physical characterization was primarily performed on the two L peptides as no significant nanostructure changes would be expected when all L amino acids on self-assembled peptides were substituted by D-amino acids [42, 43].

3.2 Characterization of nanostructure

As discussed above, due to excess of positive charges and increased electrostatic repulsion, K10 is expected to form nanofibers in a shorter dimension than that of K6 under the physiological condition, which has been confirmed by TEM (**Figure 1a** and **1b)**. A total number of 200 nanofibers were randomly selected and subject to length measurement and statistics evaluation, yielding an average diameter of nanofibers formed by K10 at ~20 nm while K6 showed bimodal distribution of fiber length at approximately 40 nm and 80 nm. As a result of the supramolecular assembly, clusters of lysine residues will be organized at the fiber-solvent interface to have multivalent interactions with the negatively charged lipid membrane. It is worth noting that although the number of charges per peptide chain varies between the two peptides, upon self-assembly the overall charges per nanofiber was estimated to be comparable, therefore eliminating

the concern of charge-dependent cell uptake. Our results show that nanofibers formed by K10 peptides are much more effective in perturbing the cell membrane as characterized by electrophysiology and cell uptake experiments. The fiber morphology is likely to impact the flexibility and orientation of the lysine residues at the N-terminus, which may be a significant factor influencing the membrane activity of FCPPs as will be discussed later.

3.3 Determination of critical assembly concentration

Critical assembly concentration (CAC) has been commonly used to evaluate the relative thermodynamic stability of amphiphilic self-assemblies. The origin of nanofiber formation is due to the balance of attractive and repulsive forces leading to equilibrium nanostructures with tunable thermodynamic stability. Increasing the number of lysine residues will increase electrostatic repulsion among peptide subunits and drive the equilibrium toward fiber dissociation. The reduction of fiber length is therefore closely related to the decreased thermodynamic stability as the number of lysine residues increases. CACs were determined using a previous protocol based on the fluorescence intensity change of tryptophan (W) that is very sensitive to the polarity of its microenvironment as a function of peptide concentration [35, 36] (**Figure S1**). At the CAC, fluorescence quenching occurs leading to a deviation of the fluorescence intensity from the trend of linear relationship between concentration and intensity. As shown in **Figure 2**, both K10 and K6 are capable of self-assembly given the non-linear relationship. The CAC value for K10 is determined at 10.1 μM while K6 is at 8.0 μM, suggesting lower thermodynamic stability of the supramolecular assembly formed by K10 than that of K6.

3.4 Kinetic stability

The kinetic stability of peptide nanofiber was investigated using our previously established fluorescence-based method [44]. Experimentally, FITC-labeled K10 or K6 (~15 μM) were

assembled in aqueous solution leading to fluorescence self-quenching. Non-labeled peptides were added to the labeled peptide solution at a molar ratio of 40:1. Due to peptide subunit exchange between labeled and non-labeled nanofibers, fluorescence intensity of self-quenched FITC was recovered. The relative fluorescence intensity change as a function of time can be used as a measure of the rate of exchange kinetics. Figure **S2** shows the fitting of the fluorescence recovery data into the following first-order kinetics equation with two disassociation rate constants.

$$I(t) = I(\infty)+[I(0)-I(\infty)]\text{x}[fe^{-k_1 t}+(1-f)\, e^{-k_2 t}]$$

The fast rate constant, k_1 accounts for the dilution effect of labeled nanofibers upon addition of non-labeled ones. The slower rate constant, k_2 represents the rate of monomer dissociation from labeled peptide nanofibers followed by rapid incorporation into non-labeled nanofibers (due to its large excess) and was used to compare the kinetics stability of different assemblies. $I(\infty)$ refers to the fluorescence intensity of the equilibrium system where labeled peptides are "diluted" in the non-labeled peptide nanofibers to a maximum extent to complete inhibit the self-quenching effect. However, $I(\infty)$ is difficult to measure experimentally due to slow exchange kinetics of the nanofiber assembly. Therefore, we used the fluorescence intensity of a FITC-tagged monomeric MDP to represent $I(\infty)$ in the fitting process. The results suggest both assemblies undergo slow exchange kinetics ($7.8\text{x}10^{-6}$ min^{-1} for K10 and $3.8\ \text{x}10^{-6}$ min^{-1} for K6) and being kinetically stable as long-circulating nanocarriers although peptide subunits are more labile within K10 nanofiber than those in K6.

3.5 Membrane activity through patch-clamp electrophysiology characterization

The ability of K10 and K6 to perturb the cell membrane was first investigated through patch clamp electrophysiology in HEK293 cell line. In this experiment, K10 was adjusted to 16 μM and K6 to 26 μM (both above their CACs) to have equal amounts of cationic charges on the

peptides. *Tr*ansmembrane current was measured in a single cell patched voltage-clamp configuration with a constant transmembrane voltage at -40 mV. Upon exposure of the patched HEK293 cell to K10, substantial and irreversible current leakage was detected (**Figure 3a**), suggesting membrane destabilization and pore formation. The time delay for current leakage is presumably due to initial contact and structural organization of K10 on the cell membrane required for effective membrane perturbation. Under the same experimental condition, HEK293 cells showed much slower response to the addition of K6 with an average current leakage onset at 52.80 s (±21.03), compared to 9.233 s (±1.967) for K10 ($p=0.0320$) (**Figure 3b**). The different membrane activity is correlated with the structural organization of each peptide on both the molecular and supramolecular level. Nanofibers formed by K6 and K10 are expected to have comparable amounts of charges as the extended length of K6 nanofiber compensated for the less numbers of lysine residues per peptide. K6 and K10 differ in their secondary structure and fiber morphology. Both peptides consist of a central beta-sheet forming domain that self-assembled into what is considered to be a "rigid" supramolecular fiber backbone. The charge domain is designed to counterbalance such rigidity through electrostatic repulsion to afford flexibility to both the molecular structure and supramolecular nanostructure and further tune the length of the nanofiber. Conceivably, in the design of self-assembled MDPs, short nanofibers are comprised of charge domains that are more flexible than those in elongated nanofibers. The correlation between fiber length and secondary structure and their flexibility was confirmed by circular dichroism (CD) spectroscopy and TEM. CD showed K6 adopts a more defined, therefore rigid beta-sheet secondary structure than K10 with a mixed beta-sheet and random coil (**Figure S3**). TEM demonstrated that supramolecular nanofibers formed by K6 appear to be more rod-like while K10 formed flexible worm-like nanofibers in shorter dimension. Potent membrane perturbation may

require supramolecular assemblies that are in an ideal balance between fiber morphology and secondary structure flexibility. The nanofiber formed by K10 represents an excellent example to be used to probe such structure-activity correlation for new types of supramolecular cell penetrating materials.

3.6 Cell uptake of Nanofibers

Extended cell exposure to supramolecular peptides and the effect of fiber morphology on cell uptake was studied by confocal laser scanning microscopy (CLSM) and flow cytometry. Generally, peptide stock solution (~ 400 μM) was prepared in a salt-free Tris buffer (20 mM, pH=7.4) for long-term storage and the concentration of each peptide was accurately determined based on the UV absorption of tryptophan. Dilution was made in cell culture media to achieve desired concentrations. For the cell uptake experiment, both peptides were diluted to a final concentration of 16 μM to have the same numbers of fluorescein molecules on peptides for the comparison of their uptake efficiency. The integrity of peptide nanofiber in the presence of serum and other enzymes is the key to their function. For the family of MDPs, previously we have thoroughly investigated their serum stability and their resistance to trypsin, alpha-chymotrypsin and DNAse I (upon encapsulation with plasmids for transfection), and the results confirmed strong resistance of self-assembled peptides to enzymatic degradation [31-33]. FITC-labeled K10 and K6 were incubated with HeLa cells for 2 hrs and 24 hrs for direct comparison of time-dependent cell uptake and localization. As shown **in Figure 4a**, after 2 hrs of incubation, both K6 and K10 were localized on the cell membrane. Further incubation of K10 with HeLa cells for 24 hrs allowed the peptide to escape from the membrane region and resulted in substantial cell internalization. Co-localization of peptides (in green) with lysotracker Red DND-99 suggests an endocytosis pathway involved for cell uptake of K10. In contrast, the majority of K6 still localized on the cell membrane

although the peptide appeared to be more diffuse into the intracellular region after 24 hrs of incubation. The distinct cell localization exhibited by K10 and K6 suggests the important role of fiber morphology and structural flexibility in mediating their interaction with the cell membrane and cell uptake. Both peptides initially bind to the negatively charged lipid membrane, however, K10 nanofiber due to its charge flexibility may be more effective to deform the cell membrane and induce endocytosis for cell internalization [45]. The longer and more rigid nanofiber formed by K6 lacks the flexibility necessary for effective membrane interaction and receptor-mediated endocytosis, therefore leading to accumulation of peptides on the cell membrane. The effect of supramolecular nanostructure on cell uptake was quantitatively studied by flow cytometry. As demonstrated in **Figure 4b**, K10 showed much higher cell uptake than K6 at both 2 hrs and 24 hrs time points. Notably, the fluorescence intensity of HeLa cells upon treatment of K10 for 2 hrs was greater than that of K6 upon incubation for 24 hrs. Statistical measurements of time-dependent fluorescence intensity (**Figure 4c**) exhibited increased cell uptake for both peptides at 24 hrs compared to that at 2 hrs. The change of fluorescence intensity was found to be more dramatic for K10 than K6.

3.7 In vitro cytotoxicity enhancement study

A goal for nanocarriers development is their potency to cross the cell membrane for highly effective intracellular delivery of a variety of membrane impermeable cargos. The exceptional membrane perturbation ability and cell penetration activity exhibited by K10 provided great impetus for us to explore their potential as highly effective therapeutics delivery vehicles or simply chemotherapeutic enhancers *in vitro*. As a model drug, water soluble, membrane impermeable Doxorubicin (DOX, in the form of HCl salt) was used to test the ability of the nanofiber formed by K10 and K6 to facilitate DOX uptake for improved *in vitro* therapeutic efficacy. The hypothesis

is that membrane defects caused by K10 nanofiber will allow DOX to penetrate through the cell membrane to induce cell death at a relatively low dosage. In this experiment, DOX and peptides were physically mixed in cell culture medium without covalent linkage or specifically designed non-covalent interaction between the two components in the formulation. The lack of physical interactions between DOX and peptides was confirmed by fluorescence spectroscopy of DOX showing minimal change of the emission peak upon addition of peptides (data not shown). It is worth noting that the focus of current study is to validate the structure-activity correlation of designed self-assembled peptide nanofibers. For more practical *in vivo* therapeutics delivery application, DOX can be readily attached on the peptides through covalent linkage to achieve desired therapeutic efficacy.

Experimentally, three formulations were prepared for *in vitro* anticancer drug efficacy test. The control group has HeLa cells incubated with DOX alone, while the test groups contain DOX mixed with either 16 μM of K10 or 26 μM of K6 in the cell culture. After 1, 8 and 24 hrs, DOX and peptides were removed from the cell culture for CCK8 cell viability assay. The viability results for the three formulations at various time points were shown in **Figure 5**. After 1 hr of incubation (**Figure 5a**), all formulations have minimal effect on cell viability. After 8 hrs, HeLa cell viability was greatly reduced upon treatment of K10+DOX compared to K6+DOX and DOX alone at all tested drug concentrations (1 μM, 10 μM, and 100 μM) (**Figure 5b**). Cell viability continued to decrease upon further incubation of cells with all three formulations although K10 was found to be the most effective in killing cells at all DOX concentrations (**Figure 5c**). We believe the enhanced cytotoxicity is largely due to the ability of K10 to perturb the cell membrane to facilitate cell uptake of DOX as K10 and K6 exhibited negligible cytotoxicity toward HeLa cells (**Figure S4**). The mechanistic origin for enhanced cytotoxicity observed here is clearly distinct from studies

where improved therapeutic efficacy was achieved through synergistic effect of multiple small molecule anticancer/antimicrobial drugs and synthetic macromolecules [46-50]. Notably, K10 was found to be more effective to enhance the therapeutic efficacy of DOX at a lower drug dosage. For example, as shown in **Figure 5c**, after 24 hrs of incubation, although cell viability of the three groups is comparable at 100 μM of DOX, the cytotoxicity effect was dramatically different at 1 μM of DOX with K10 treated group at 22% in comparison to 57% for the K6 group and 70% for the control group. More impressively, with the addition of K10, 1 μM of DOX have comparable levels of cell viability (22%) to that of DOX alone at 100 μM (18%). These results indicated that with the peptide nanofiber formulation, very limited amounts of DOX was needed to achieve desired anticancer drug efficacy while traditional chemotherapy often requires much higher dosage of drugs for effective treatment but accompanied with lots of side effects. We performed IC50 measurements for free DOX and DOX in the presence of K10. Based on the results (**Figure S5**), IC50 of DOX in the presence of K10 was estimated at 0.5 μM which is eight times less than that of free DOX at 4 μM, further confirming the chemotherapeutic enhancement effect of the K10 nanofiber.

To further study peptide-induced toxicity enhancement effect, CLSM was used to monitor time-dependent cell uptake of DOX with or without peptides. As shown in **Figure S6**, very limited DOX uptake was found for both K10 and K6 treated cell culture after 2 hrs of incubation. After 8 hrs, cells incubated with K10 showed much stronger florescence than K6 treated group, which accounts for lower cell viability results observed for K10+DOX compared to that of K6+DOX formulation and the control group.

To exclude the possibility of enzymatic degradation and possible tracking of only the dye molecule in the *in vitro* experiment, D amino acid containing peptide was synthesized to have the

same sequence of K10. As shown in **Figure S7** and **6**, the D peptide (labeled as ^{d}K10 in Figure **6**) showed similar cell uptake profile and toxicity enhancement effect compared to its L nanofibers, which validates the design principle of nanostructure-controlled membrane activity observed in the L-peptide systems.

4. Conclusions

In summary, we have demonstrated the design of a new class of supramolecular peptide nanofiber with tunable molecular structure and supramolecular nanostructure. Cellular interaction of two peptide nanofibers was thoroughly investigated by patch-clamp electrophysiology and confocal microscopy yielding important information about supramolecular structure dependent membrane activity. Nanofibers were found to sacrifice their dimension, thermodynamic and kinetic stability for a more flexible charge domain in order to achieve effective membrane interaction. By taking advantage of the exceptional membrane activity of K10 nanofibers, we showed optimal *in vitro* anticancer drug efficacy by coadministering K10 and DOX at a very low dosage. The development of membrane-active supramolecular nanofibers and fundamental understanding of their structure-dependent membrane interaction will have broader impacts on nanotherapeutics design and will greatly aid in the design of supramolecular assemblies with intrinsic cell penetrating activity to achieve optimal *in vitro* and *in vivo* therapeutics efficacy.

Acknowledgments

This study was supported by the National Science Foundation (DMR 1654426). The authors would like to thank Michael Tighe of the Imaging Core at Trudeau Institute for excellent technical support of flow cytometry.

References

[1] T. Aida, E.W. Meijer, S.I. Stupp, Functional supramolecular polymers, Science 335 (2012) 813-817.
[2] S. Zhang, Fabrication of Novel biomaterials through molecular self-assembly, Nat. Biotechnol. 21 (2003) 1171-1178.
[3] R.S. Tu, M. Tirrell, Bottom-up design of biomimetic assemblies, Adv. Drug Deliv. Rev. 56 (2004) 1537-1563.
[4] S. Rele, Y. Song, R.P. Apkarian, Z. Qu, V.P. Conticello, E.L. Chaikof, D-periodic collagen-mimetic microfibers, J. Am. Chem. Soc. 129 (2007) 14780-14787.
[5] C. Yan, D.J. Pochan, Rheological properties of peptide-based hydrogels for biomedical and other applications, Chem. Soc. Rev. 39 (2010) 3528-40.
[6] C.E. Morgan, A.W. Dombrowski, C.M. Rubert Pérez, E.S.M. Bahnson, N.D. Tsihlis, W. Jiang, Q. Jiang, J.M. Vercammen, V.S. Prakash, T.A. Pritts, S.I. Stupp, M.R. Kibbe, Tissue-factor targeted peptide amphiphile nanofibers as an injectable therapy to control hemorrhage, ACS Nano 10 (2016) 899-909.
[7] A.G. Cheetham, P. Zhang, Y.-a. Lin, L.L. Lock, H. Cui, Supramolecular nanostructures formed by anticancer drug assembly, J. Am. Chem. Soc. 135 (2013) 2907-2910.
[8] C.J. Newcomb, S. Sur, J.H. Ortony, O.-S. Lee, J.B. Matson, J. Boekhoven, J.M. Yu, G.C. Schatz, S.I. Stupp, Cell death versus cell survival instructed by supramolecular cohesion of nanostructures, Nat. Commun. 5 (2014) 3321.
[9] J. Zhou, X. Du, N. Yamagata, B. Xu, Enzyme-instructed self-assembly of small D-peptides as a multiple-step process for selectively killing cancer cells, J. Am. Chem. Soc. 138 (2016) 3813-3823.
[10] J.S. Rudra, Y.F. Tian, J.P. Jung, J.H. Collier, A self-assembling peptide acting as an immune adjuvant, Proc. Natl. Acad. Sci. U.S.A. 107 (2010) 622-627.
[11] V.A. Kumar, N.L. Taylor, S. Shi, N.C. Wickremasinghe, R.N. D'Souza, J.D. Hartgerink, Self-assembling multidomain peptides tailor biological responses through biphasic release, Biomaterials 52 (2015) 71-8.
[12] M.T. McClendon, S.I. Stupp, Tubular hydrogels of circumferentially aligned nanofibers to encapsulate and orient vascular cells, Biomaterials 33 (2012) 5713-5722.
[13] V.A. Kumar, Q. Liu, N.C. Wickremasinghe, S. Shi, T.T. Cornwright, Y. Deng, A. Azares, A.N. Moore, A.M. Acevedo-Jake, N.R. Agudo, S. Pan, D.G. Woodside, P. Vanderslice, J.T. Willerson, R.A. Dixon, J.D. Hartgerink, Treatment of hind limb ischemia using angiogenic peptide nanofibers, Biomaterials 98 (2016) 113-119.
[14] S. Koutsopoulos, S. Zhang, Long-term three-dimensional neural tissue cultures in functionalized self-assembling peptide hydrogels, matrigel and collagen I, Acta Biomater. 9 (2013) 5162-5169.
[15] W. Liyanage, K. Vats, A. Rajbhandary, D.S.W. Benoit, B.L. Nilsson, Multicomponent dipeptide hydrogels as extracellular matrix-mimetic scaffolds for cell culture applications, Chem. Commun. 51 (2015) 11260-11263.
[16] K.M. Galler, L. Aulisa, K.R. Regan, R.N. D'Souza, J.D. Hartgerink, Self-assembling multidomain peptide hydrogels: Designed susceptibility to enzymatic cleavage allows enhanced cell migration and spreading, J. Am. Chem. Soc. 132 (2010) 3217-3223.
[17] M.C. Giano, D.J. Pochan, J.P. Schneider, Controlled biodegradation of Self-assembling β-hairpin peptide hydrogels by proteolysis with matrix metalloproteinase-13, Biomaterials 32 (2011) 6471-6477.

[18] X. Huang, L. Li, T. Liu, N. Hao, H. Liu, D. Chen, F. Tang, The shape effect of mesoporous silica nanoparticles on biodistribution, clearance, and biocompatibility in vivo, ACS Nano 5 (2011) 5390-5399.
[19] H. Jin, D.A. Heller, R. Sharma, M.S. Strano, Size-dependent cellular uptake and expulsion of single-walled carbon nanotubes: Single particle tracking and a generic uptake model for nanoparticles, ACS Nano 3 (2009) 149-158.
[20] B.D. Chithrani, A.A. Ghazani, W.C.W. Chan, Determining the size and shape dependence of gold nanoparticle uptake into mammalian cells, Nano Lett. 6 (2006) 662-668.
[21] A.M. Alkilany, P.K. Nagaria, C.R. Hexel, T.J. Shaw, C.J. Murphy, M.D. Wyatt, Cellular uptake and cytotoxicity of gold nanorods: molecular origin of cytotoxicity and surface effects, Small 5 (2009) 701-708.
[22] Y. Geng, P. Dalhaimer, S. Cai, R. Tsai, M. Tewari, T. Minko, D.E. Discher, Shape effects of filaments versus spherical particles in flow and drug delivery, Nat. Nanotechnol. 2 (2007) 249-255.
[23] H. Cao, X. Jiang, C. Chai, S.Y. Chew, RNA interference by nanofiber-based siRNA delivery system, J. Control. Release 144 (2010) 203-212.
[24] S.E. Gratton, P.A. Ropp, P.D. Pohlhaus, J.C. Luft, V.J. Madden, M.E. Napier, J.M. DeSimone, The effect of particle design on cellular internalization pathways, Proc. Natl. Acad. Sci. U.S.A. 105 (2008) 11613-11618.
[25] C. He, Y. Hu, L. Yin, C. Tang, C. Yin, Effects of particle size and surface charge on cellular uptake and biodistribution of polymeric nanoparticles, Biomaterials 31 (2010) 3657-3666.
[26] S. Sim, T. Niwa, H. Taguchi, T. Aida, Supramolecular nanotube of chaperonin GroEL: Length control for cellular uptake using single-ring GroEL mutant as end-capper, J. Am. Chem. Soc. 138 (2016) 11152-11155.
[27] S. Biswas, K. Kinbara, T. Niwa, H. Taguchi, N. Ishii, S. Watanabe, K. Miyata, K. Kataoka, T. Aida, Biomolecular robotics for chemomechanically driven guest delivery fuelled by intracellular ATP, Nat. Chem. 5 (2013) 613-620.
[28] Y. Ma, R.J.M. Nolte, J.J.L.M. Cornelissen, Virus-based nanocarriers for drug delivery, Adv. Drug Deliv. Rev. 64 (2012) 811-825.
[29] M.L. Becker, J.A. Fagan, N.D. Gallant, B.J. Bauer, V. Bajpai, E.K. Hobbie, S.H. Lacerda, K.B. Migler, J.P. Jakupciak, Length-dependent uptake of DNA-wrapped single-walled carbon nanotubes, Adv. Mater. 19 (2007) 939-945.
[30] J.J. Cronican, D.B. Thompson, K.T. Beier, B.R. McNaughton, C.L. Cepko, D.R. Liu, Potent delivery of functional proteins into Mammalian cells in vitro and in vivo using a supercharged protein, ACS Chem. Biol. 5 (2010) 747-52.
[31] D. Xu, D. Dustin, L. Jiang, D.S.K. Samways, H. Dong, Designed filamentous cell penetrating peptides: Probing supramolecular structure-dependent membrane activity and transfection efficiency, Chem. Commun. 51 (2015) 11757-11760.
[32] D. Xu, L. Jiang, A. Singh, D. Dustin, M. Yang, L. Liu, R. Lund, T.J. Sellati, H. Dong, Designed supramolecular filamentous peptides: Balance of nanostructure, cytotoxicity and antimicrobial activity, Chem. Commun. 51 (2015) 1289-1292.
[33] M. Yang, D. Xu, L. Jiang, L. Zhang, D. Dustin, R. Lund, L. Liu, H. Dong, Filamentous supramolecular peptide-drug conjugates as highly efficient drug delivery vehicles, Chem. Commun. 50 (2014) 4827-4830.

[34] D. Xu, L. Jiang, L. DeRidder, B. Elmore, M. Bukhari, Q. Wei, D.S.K. Samways, H. Dong, Membrane activity of a supramolecular peptide-based chemotherapeutic enhancer, Mol. Biosyst. 12 (2016) 2695-2699.
[35] D. Xu, Q. Ran, Y. Xiang, L. Jiang, B.M. Smith, F. Bou-Abdallah, R. Lund, Z. Li, H. Dong, Toward Hemocompatible Self-assembling antimicrobial nanofibers: Understanding the synergistic effect of supramolecular structure and PEGylation on hemocompatibility, RSC Adv. 6 (2016) 15911-15919.
[36] Y. Chen, M.D. Barkley, Toward understanding tryptophan fluorescence in proteins, Biochemistry 37 (1998) 9976-9982.
[37] M. Cahalan, E. Neher, Patch clamp techniques: an overview, Methods Enzymol. 207 (1992) 3-14.
[38] H. Dong, S.E. Paramonov, L. Aulisa, E.L. Bakota, J.D. Hartgerink, Self-assembly of multidomain peptides: Balancing molecular frustration controls conformation and nanostructure, J. Am. Chem. Soc. 129 (2007) 12468-12472.
[39] H. Dong, N. Dube, J.Y. Shu, J.W. Seo, L.M. Mahakian, K.W. Ferrara, T. Xu, Long-circulating 15 nm micelles based on Aamphiphilic 3-helix peptide–PEG conjugates, ACS Nano 6 (2012) 5320-5329.
[40] CabralH, MatsumotoY, MizunoK, ChenQ, MurakamiM, KimuraM, TeradaY, M.R. Kano, MiyazonoK, UesakaM, NishiyamaN, KataokaK, Accumulation of sub-100 nm polymeric micelles in poorly permeable tumours depends on size, Nat. Nanotechnol. 6 (2011) 815-823.
[41] Z. Popović, W. Liu, V.P. Chauhan, J. Lee, C. Wong, A.B. Greytak, N. Insin, D.G. Nocera, D. Fukumura, R.K. Jain, M.G. Bawendi, A nanoparticle size series for in vivo fluorescence imaging, Angew. Chem. Int. Ed. 49 (2010) 8649-8652.
[42] X. Li, X. Du, J. Li, Y. Gao, Y. Pan, J. Shi, N. Zhou, B. Xu, Introducing D-amino acid or simple glycoside into small peptides to enable supramolecular hydrogelators to resist proteolysis, Langmuir 28 (2012) 13512-13517.
[43] J. Shi, X. Du, D. Yuan, J. Zhou, N. Zhou, Y. Huang, B. Xu, D-amino acids modulate the cellular response of enzymatic-instructed supramolecular nanofibers of small Peptides, Biomacromolecules 15 (2014) 3559-3568.
[44] H. Dong, J.Y. Shu, N. Dube, Y. Ma, M.V. Tirrell, K.H. Downing, T. Xu, 3-Helix micelles stabilized by polymer springs, J. Am. Chem. Soc. 134 (2012) 11807-11814.
[45] W.W. Yau, H. Long, N.C. Gauthier, J.K. Chan, S.Y. Chew, The effects of nanofiber diameter and orientation on siRNA uptake and gene silencing, Biomaterials 37 (2015) 94-106.
[46] Y. Cai, H. Shen, J. Zhan, M. Lin, L. Dai, C. Ren, Y. Shi, J. Liu, J. Gao, Z. Yang, Supramolecular "Trojan Horse" for nuclear delivery of dual anticancer drugs, J. Am. Chem. Soc. 139 (2017) 2876-2879.
[47] Y. Wang, X.Y. Ke, J.S. Khara, P. Bahety, S. Liu, S.V. Seow, Y.Y. Yang, P.L. Ee, Synthetic modifications of the immunomodulating peptide thymopentin to confer anti-mycobacterial activity, Biomaterials 35 (2014) 3102-3109.
[48] J.S. Khara, Y. Wang, X.-Y. Ke, S. Liu, S.M. Newton, P.R. Langford, Y.Y. Yang, P.L.R. Ee, Anti-mycobacterial activities of synthetic cationic alpha-helical peptides and their synergism with rifampicin, Biomaterials 35 (2014) 2032-2038.
[49] N. Wiradharma, U. Khoe, C.A. Hauser, S.V. Seow, S. Zhang, Y.Y. Yang, Synthetic cationic amphiphilic alpha-helical peptides as antimicrobial agents, Biomaterials 32 (2011) 2204-2212.

[50] H. Lu, J. Wang, Z. Song, L. Yin, Y. Zhang, H. Tang, C. Tu, Y. Lin, J. Cheng, Recent advances in amino acid N-carboxyanhydrides and synthetic polypeptides: Chemistry, aelf-assembly and biological applications, Chem. Commun. 50 (2014) 139-155.

Figure caption

Figure 1. TEM images of the nanofibers formed by (a) K10 and (b) K6 and statistical measurements of fiber length and length distribution based on a total number of 200 fibers. Peptide concentration: 100 μM in Tris buffer (20 mM, pH = 7.4). Scale bar: 100 nm.

Figure 2. CAC determination through fluorescence measurements of peptides as a function of concentration in Tris buffer (20 mM, pH 7.4) (a) K10 and (b) K6.

Figure 3. (a) Cell membrane current change upon cell exposure to 16 μM of K10 or 26 μM of K6 for duration of 95 seconds. (b) Statistical measurements of the onset of current leakage. Data are presented as the mean ± SEM. Statistically significant differences are indicated by *$p \leq 0.05$.

Figure 4. Cell uptake of FITC-labeled K10 and K6 upon incubation with HeLa cells. (a) MDP localization after incubation with HeLa cells, Scale bar: 10 μm (b) Time-dependent cell uptake of MDPs monitored by flow cytometry after 2 hrs and 24 hrs of incubation with HeLa cell. Data are presented as the mean ± SD, n = 4. Statistically significant differences are indicated by **$p \leq 0.01$, *$p \leq 0.05$. K10: 16 μM. K6: 16 μM.

Figure 5. Hela cell viability upon incubation with DOX at different concentrations in the presence and absence of peptide nanofibers for (a) 1 hr, (b) 8 hrs and (c) 24 hrs. Data are presented as the mean ± SD, n = 4. Statistically significant differences are indicated by **$p \leq 0.01$, *$p \leq 0.05$. K10: 16 μM. K6: 26 μM.

Figure 6. Effect of peptide stereochemistry on cytotoxicity enhancement of DOX after 24 hrs of incubation with HeLa cells. Data are presented as the mean ± SD, n = 4. The final concentrations of both peptides are 16 μM.

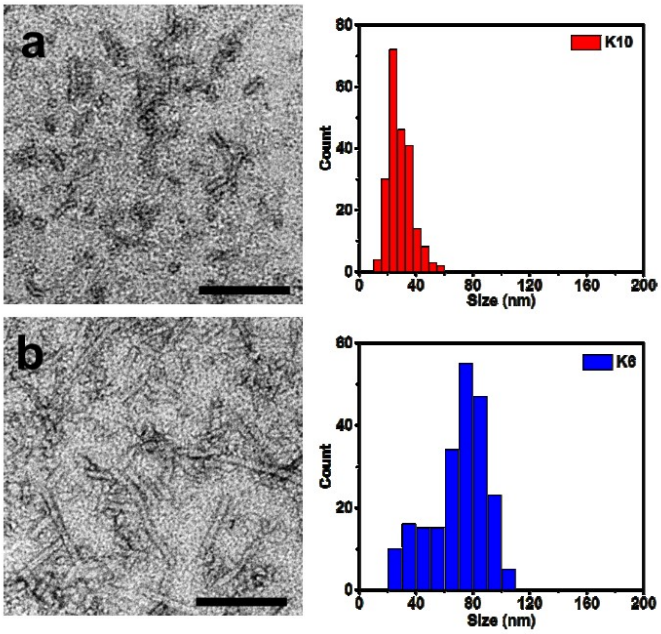

Figure 1. TEM images of the nanofibers formed by (a) K10 and (b) K6 and statistical measurements of fiber length and length distribution based on a total number of 200 fibers. Peptide concentration: 100 μM in Tris buffer (20 mM, pH = 7.4). Scale bar: 100 nm.

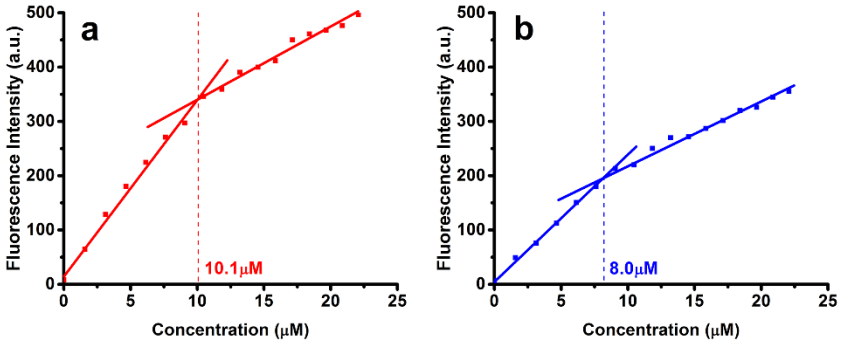

Figure 2. CAC determination through fluorescence measurements of peptides as a function of concentration in Tris buffer (20 mM, pH 7.4) (a) K10 and (b) K6.

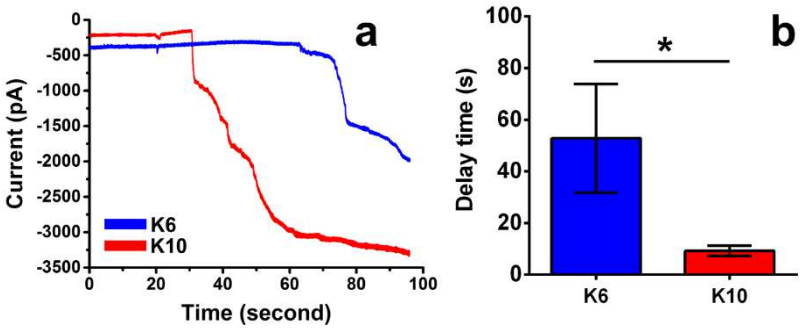

Figure 3. (a) Cell membrane current change upon cell exposure to 16 μM of K10 or 26 μM of K6 for duration of 95 seconds. (b) Statistical measurements of the onset of current leakage. Data are presented as the mean ± SEM. Statistically significant differences are indicated by *$p \leq 0.05$.

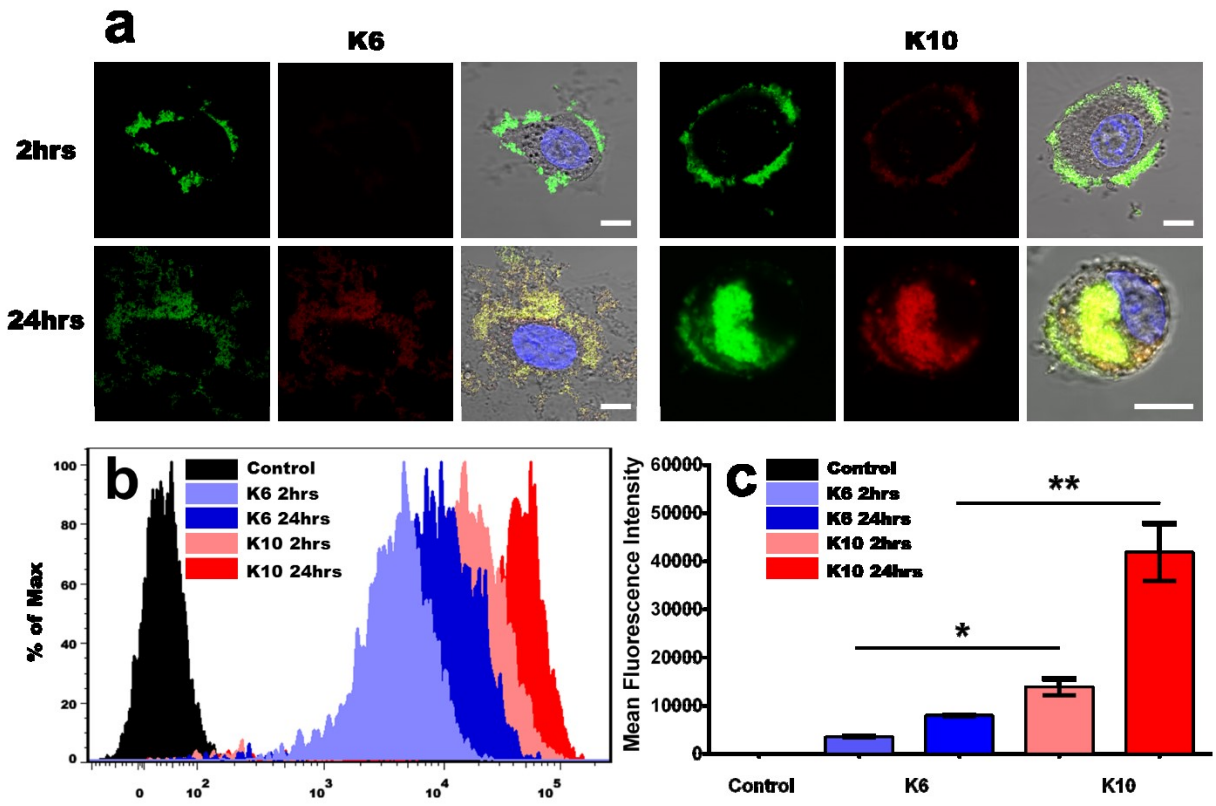

Figure 4. Cell uptake of FITC-labeled K10 and K6 upon incubation with HeLa cells. (a) MDP localization after incubation with HeLa cells, Scale bar: 10 μm (b) Time-dependent cell uptake of MDPs monitored by flow cytometry after 2 hrs and 24 hrs of incubation with HeLa cell. Data are presented as the mean ± SD, n = 4. Statistically significant differences are indicated by $^{**}p \leq 0.01$, $^{*}p \leq 0.05$. K10: 16 μM. K6: 16 μM.

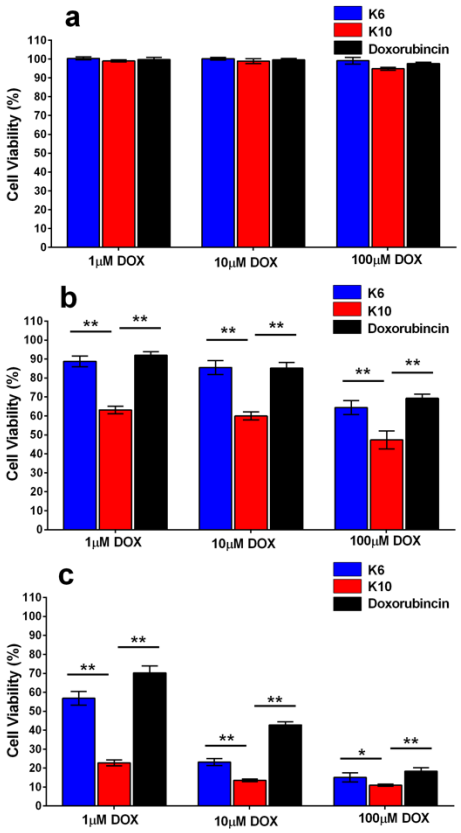

Figure 5. Hela cell viability upon incubation with DOX at different concentrations in the presence and absence of peptide nanofibers for (a) 1 hr, (b) 8 hrs and (c) 24 hrs. Data are presented as the mean ± SD, n = 4. Statistically significant differences are indicated by **p ≤ 0.01, *p ≤ 0.05. K10: 16 μM. K6: 26 μM.

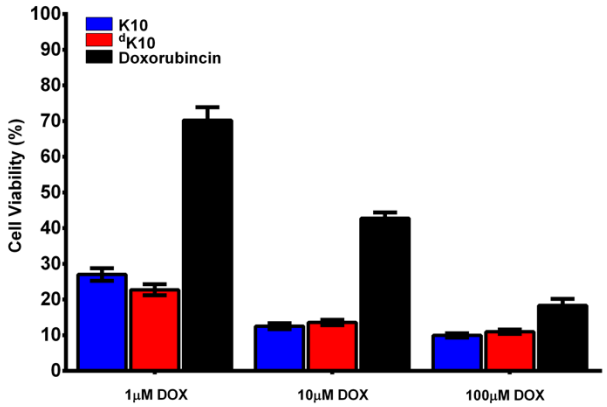

Figure 6. Hela cell viability upon incubation with DOX in the presence and absence of peptide nanofibers with different stereochemistry for 24 hrs. Data are presented as the mean ± SD, n = 4. The final concentrations of both peptides are 16 μM.